

## GMRES Computation of High Frequency Electrical Field Propagation in Land Mine Detection

Yuriy A. Gryazin,<sup>\*,†</sup> Michael V. Klibanov,<sup>\*</sup> and Thomas R. Lucas<sup>\*</sup>

<sup>\*</sup>*Department of Mathematics, University of North Carolina at Charlotte, Charlotte, North Carolina 28223;*

<sup>†</sup>*Institute of Computational Technologies, Novosibirsk, 630090, Russia*

E-mail: {ygryazin,mvklibanv,trlucas}@uncc.edu

Received June 21, 1999; revised November 1, 1999

The ultimate goal of the authors is to apply inverse problem techniques to image land mines using an electromagnetic signal originated by ground penetrating radar. Specifically, the intention is to use the recently developed elliptic systems method, which has been successfully applied by these authors to the problem of imaging biological tissues using lasers. As the first step it is necessary to develop a fast and accurate numerical method for the solution of the forward problem to simulate data for the inverse problem. The main challenge is the requirement of solving a Helmholtz-like equation for *high* frequencies which is excessively time consuming using standard direct solution techniques. A novel accurate and rapid numerical procedure for the solution of this equation is described in this paper. The kernel of this algorithm is a combination of GMRES and a carefully chosen preconditioner, the solution of which is found using a fast transform method. The extended problem of solving Helmholtz-like equations for many frequencies is also considered. Numerical results for realistic ranges of parameters in soil and mine-like targets, the investigation of the impact of the size of the truncation region on accuracy, and the sensitivity of detector readings to changes in the media are presented. © 2000 Academic Press

**Key Words:** land mines; Helmholtz equation; elliptic systems method; GMRES.

### 1. INTRODUCTION

The goal of this paper is to describe a novel and effective numerical method for the forward solution of high frequency electromagnetic wave propagation. This method will be used later by the authors to computationally simulate data for the solution of the inverse problem of imaging mine-like targets using the elliptic systems method [10, 19, 20]. Thus the solution of the forward problem presented in this paper is a necessary prelude to the future solution of a related inverse problem.



20000523 088

The problem of imaging land mines is of great significance. Handheld ground penetrating radars (GPRs) represent a non-expensive hardware device for this purpose. A principal difficulty of GPRs, however, is linked with a high percentage of false alarms, as well as false negatives; the latter especially relates to plastic mines.

Land mines are modeled as small abnormalities imbedded in an otherwise uniform media with an air-ground interface. These abnormalities are characterized by the electrical permittivity  $\varepsilon$  and the conductivity  $\sigma$ , whose values differ from those of the host media. The inverse problem consists of the determination of perturbations in  $\varepsilon$  and  $\sigma$ , using measurements of output electrical signals at a number of angular frequencies  $\omega$  and at a number of detectors (i.e., antennas) located near the ground surface. These perturbations of the electrical parameters will be used to characterize both locations of mine-like targets and to differentiate mines from clutter.

However, as is always the case in inverse problems, it is first necessary to solve the forward problem in order to simulate the data for the inverse problem. Two important requirements for the forward solver are: (1) it should be accurate, and (2) it should be fast. The importance of the second requirement is due to the practical necessity of conducting a large number of numerical tests of the inverse algorithm. The main difficulty in solving the forward problem is that it must be solved for large values of the angular frequencies, i.e., for small wave lengths. Thus a large number of grid points must be used. In this paper we present a novel numerical method for the solution of the forward problem, which satisfies the above two requirements.

The problem considered in this paper is to compute the numerical solution of the Helmholtz equation

$$\nabla^2 v + k^2(x, y)v = f, \quad \text{in } \Omega \quad (1.1)$$

with the Sommerfeld-like boundary conditions

$$v_n - ikv = 0, \quad \text{on } \partial\Omega, \quad (1.2)$$

where  $\Omega = \{-a \leq x, y \leq a\}$ ; and  $k^2$ ,  $v$ , and  $f$  are complex valued functions. Equation (1.2) represents an absorbing boundary condition which allows normally incident waves to pass out of  $\Omega$  transparently. It is implicitly assumed that the support of  $f$  lies well inside the interior of  $\Omega$ .

If the problem is discretized using a second order centered finite-difference scheme on a regular mesh, the resulting linear system of equations has block tridiagonal structure. This matrix is neither positive definite nor Hermitian. Hence, most iterative methods either fail to converge or converge too slowly, which is impractical. Concerning the other approaches for the solution of the problem (1.1)–(1.2), we refer to Bayliss *et al.* [1] for a preconditioned conjugate-gradient algorithm, Despres [7] and Kim [17, 18] for a domain decomposition method, and Douglas *et al.* [9] for an ADI algorithm.

The application of multilevel methods suffers from the requirement that the coarse meshes used must be fine enough to accurately represent the solution; see [3]. On the other hand the solution of this problem by a direct method based on Gaussian elimination requires a prohibitive amount of additional storage and computer time and thus has limited use. The most promising results in the solution of a similar problem have been obtained by preconditioned Krylov subspace methods [12, 14, 16]. In this paper we generalize some

approaches developed for the Helmholtz equation with constant coefficients by Ernst and Golub [14] and Elman and O'Leary [12]. In these papers the authors derived an excellent preconditioner by replacing the Sommerfeld-like boundary conditions with Dirichlet or Neumann boundary conditions. They presented numerical experiments which demonstrated that their preconditioner had good convergence properties. However, their problem, unlike the one of this paper, did not involve interfaces or additional heterogeneities such as land mines or other small abnormalities.

A key question concerning the choice of a preconditioner when the boundary conditions are different from those of the original problem is the influence of this discrepancy on the convergence of the corresponding iterative algorithm. Manteuffel and Parter [21] and Joubert *et al.* [15] have proven interesting results about a problem similar to ours. In particular, they have proven that if both the preconditioner  $B_h$  and the given operator  $A_h$  are discretizations of second-order elliptic operators  $A$  and  $B$ , then the  $L_2$  condition number of the preconditioned problem  $A_h B_h^{-1}$  is bounded and the bound is independent of  $h$  if and only if  $B$  and  $A$  have the same boundary conditions. Similarly, the  $L_2$  condition number of the operator  $B_h^{-1} A_h$  is bounded independently of  $h$  if and only if the adjoint problems  $B^*$  and  $A^*$  have the same boundary conditions. They have also shown that the  $H_1$  condition number of  $B_h^{-1} A_h$  is bounded independently of  $h$  if and only if  $A$  and  $B$  have Dirichlet boundary conditions on the same portion of the boundary. However, these results cannot be directly applied to estimations of convergence of GMRES-based methods (see, for example, [13, 23, 24]), because convergence in this case depends on the *distribution* of eigenvalues along with the eigenvectors of the preconditioned matrix, rather than just the condition number. In [13] Elman and O'Leary considered the spectra of the preconditioned operator in the case of the solution of the Helmholtz equation with constant coefficients and replaced Sommerfeld boundary conditions with either Dirichlet or Neuman boundary conditions in the preconditioner. They established, by direct numerical experiments, that in the case of the Neumann preconditioned matrix the eigenvalues of this matrix are bounded away from zero, which leads to the fast convergence of the algorithm. Thus, one should expect good performance of GMRES with the Neumann preconditioner in the case of non-constant coefficients as well. This expectation was confirmed in our numerical experiments.

In our numerical approach we approximate the discrete operator by a matrix operator which can be derived by the discretization of the Helmholtz equation with the coefficient  $k^2$  depending only on the  $y$  position. In this matrix operator we replace the Sommerfeld-like boundary conditions on the left and right sides with Neumann boundary conditions. Thus we keep the Sommerfeld-like boundary conditions on the top and bottom and replace the abnormalities in the media with an uniform value. The resulting matrix is then used as a preconditioner to accelerate the convergence of an iterative solver based on Krylov subspace methods. We have selected the GMRES [27] method for our accelerator. This approach requires use of the preconditioner on each GMRES iteration. This can be done by use of a fast solver which requires  $O(N^2 \log N)$  operations.

This method was presented for the first time at the SPIE "Aerosense" meeting in Orlando, in April of 1999. At the same conference a similar, but independent approach, was presented by Kilmer *et al.* [16]. They considered the application of a similar preconditioner in the case of using the QMR accelerator with perfectly matched layer (PML) boundary conditions [2] in the scattering problem for the Helmholtz equation. An important question in the problem of accurately computing the scattering field is the selection of boundary conditions, because in practical applications the actual physical domain is infinite, but as is standard, we use a

finite truncation region, with suitable boundary conditions. One currently popular technique is the use of PML boundary conditions [2]. This approach produces good results in time domain computations for the propagation of electromagnetic waves. However, in the case of the frequency domain the optimal choice of the parameters, which should be set a priori, is less clear. In this paper we use Sommerfeld-like boundary conditions instead of PML boundary conditions. The numerical implementation of Sommerfeld-like boundary conditions is easier than that of PLM, thus offering advantages if the solutions are not inferior. A natural question arises as to the quality of the numerical solution for various approaches. To evaluate the impact of our selection of boundary conditions in the context of this problem, numerical tests for computational domains of different sizes were performed. The computations tested if the solution in a fixed middle region is independent, in practice, of the size of the truncation region, when that region is of moderate size or larger.

One of the goals of this work is to investigate the application of the algorithm to the solution of problem (1.1)–(1.2) for a sequence of frequencies. Because the coefficient  $k^2(x, y)$  depends on the frequency and we implicitly make iterations with respect to this coefficient, it is to be expected that the number of iterations required for the convergence would depend on the frequency as well. To prevent or limit the growth of the number of iterations as the frequency increases we have investigated different extrapolation techniques. Using these techniques we select an initial approximation for each iteration. This procedure significantly reduces the total time required for the solution of the problem for many different frequencies.

Finally, for this work to be useful for the related inverse problem, it is necessary that changes in the distribution of coefficients of the targets (land mines) result in suitable changes in the detector values. These and other numerical results will be discussed in Section 4.

## 2. STATEMENT OF THE BOUNDARY VALUE PROBLEM

We consider the following simple mathematical model for the propagation of an electromagnetic field: Let  $(x, y, z)$  be coordinates in the 3-dimensional euclidean space  $R^3$  and  $\{y = 0\}$  be the air-ground interface. We let air be given by  $\{y < 0\}$  and the ground by  $\{y > 0\}$ . Let an electrical field  $E_0$  originated by a GPR be a linearly polarized plane wave with the direction of propagation parallel to the positive direction of the  $y$ -axis,  $E_0 = (0, 0, e^{i\omega y})$ , where  $\omega$  is the angular frequency. Figure 1 illustrates both the computational domain and initial physical problem.

We assume that the electrical field  $E$  does not depend on the  $z$ -coordinate. Then Maxwell's system implies that  $E = (0, 0, u)$  where the function  $u = u(x, y)$  satisfies the Helmholtz PDE

$$\nabla^2 u + k^2(x, y)u = 0 \quad (2.1)$$

$$k^2(x, y) = \omega^2 \mu \varepsilon(x, y) + i\omega \mu \sigma(x, y). \quad (2.2a)$$

Usually, engineers introduce the so-called "loss tangent,"

$$\tan(\delta) = \frac{\sigma}{\omega \varepsilon}. \quad (2.2b)$$

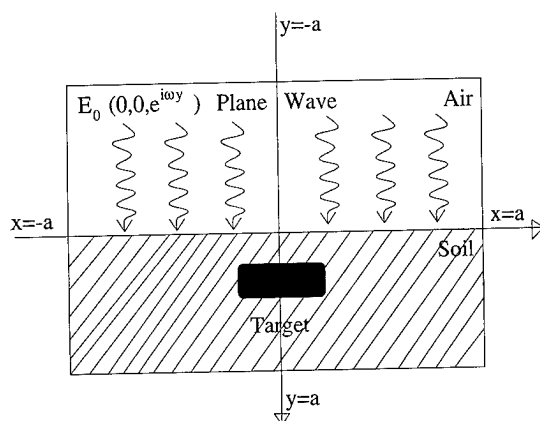


FIG. 1. Illustration of the computational domain and initial physical problem.

Substitution of (2.2b) into (2.2a) leads to

$$k^2 = \omega^2 \mu \varepsilon (1 + i \tan \delta). \quad (2.2c)$$

We assume that  $\mu \equiv \mu_0$  and  $\varepsilon = \varepsilon_0 \varepsilon_r$ , where  $\mu_0$  and  $\varepsilon_0$  are the magnetic permeability and the dielectric permittivity of a vacuum and  $\varepsilon_r$  is the relative dielectric constant. We also assume that in air, where  $y < 0$ ,  $\varepsilon = \varepsilon_0$  and  $\tan \delta = 0$ . In the ground

$$\varepsilon_r = \varepsilon_r(x, y) = \varepsilon_{r1} + \Delta \varepsilon_{r1}(x, y) > 0, \quad (2.3a)$$

$$\tan \delta = \tan[\delta(x, y)] = \tan(\delta_1) + \Delta\{\tan[\delta_1(x, y)]\}, \quad (2.3b)$$

where  $\varepsilon_{r1}$  and  $\tan(\delta_1)$  are positive constants and the perturbations  $\Delta \varepsilon_{r1}(x, y)$  and  $\Delta\{\tan[\delta_1(x, y)]\}$  are due to the presence of small mine-like targets. It is assumed that the perturbations  $\Delta \varepsilon_{r1}(x, y)$  and  $\Delta\{\tan[\delta_1(x, y)]\}$  have support only within these targets. Our method can also be generalized for a layered medium, in which case  $\varepsilon_{r1}$  and  $\tan(\delta_1)$  would be functions depending on  $y$  only. Let  $k_0 = k_0(y)$  be the function  $k(x, y)$  without inclusions present. That is,

$$k_0^2(y) = \begin{cases} \omega^2 \mu_0 \varepsilon_0, & \text{for } y < 0 \\ \omega^2 \mu_0 \varepsilon_0 \varepsilon_{r1} [1 + i \tan(\delta_1)], & \text{for } y > 0. \end{cases}$$

Hence, the function  $k_0(y)$  has constant values both in air and ground with a discontinuity at the air-ground interface. Further, let  $u_0 = u_0(x, y)$  be the solution of Eq. (2.1) which corresponds to the initializing plane wave  $e^{ik_0 y}$  ( $y < 0$ ) without inclusions present. We seek the function  $u$  in the form  $u = u_0 + v(x, y)$ , where the function  $v$  represents the wave scattered by the mine-like targets. This function satisfies the Sommerfeld boundary conditions,

$$\lim_{r \rightarrow \pm\infty} \left( \frac{\partial v}{\partial r} \mp i k v \right) = 0, \quad (2.4a)$$

where

$$\text{Im}(k) > 0. \quad (2.4b)$$

Then

$$u_0 = \begin{cases} e^{ik_0 y} + A(k_0)e^{-ik_0 y}, & \text{for } y < 0 \\ B(k_0)e^{ik_0 y}, & \text{for } y > 0, \end{cases}$$

where  $A(k_0)$  and  $B(k_0)$  are the reflection and transmission coefficients given by

$$A(k_0) = \frac{k_0^- - k_0^+}{k_0^- + k_0^+}, \quad B(k_0) = \frac{2k_0^-}{k_0^- + k_0^+}.$$

Here  $k_0^-$  and  $k_0^+$  are the values of  $k_0$  for  $y < 0$  and  $y > 0$ , respectively. The presence of these coefficients ensures the continuity of the function  $u_0$  together with its first derivatives at the air-ground interface. The uniqueness and existence results for the problem (2.1)–(2.4) were proven in [6].

Substituting  $u = u_0 + v$  into the PDE (2.1), we obtain the equation in a form which is convenient for our iterative method,

$$-\nabla^2 v - k^2 v = f, \quad (2.5a)$$

where

$$f = f(x, y, v) = \begin{cases} 0, & \text{outside inclusions,} \\ (k^2 - k_0^2)u_0, & \text{inside inclusions.} \end{cases} \quad (2.5b)$$

In our numerical algorithm we replace the infinite space  $R^2$  with a sufficiently large finite square  $\Omega = \{-a < x, y < a\}$ . We will assume below that  $k^2(x, y) = k_0^2(y)$  at the boundary of  $\Omega$ . The boundary conditions (2.4) are replaced with the Sommerfeld-like boundary conditions

$$\left( \frac{\partial v}{\partial x} \mp ikv \right) \Big|_{x=\pm a} = 0 \quad (2.6a)$$

$$\left( \frac{\partial v}{\partial y} \mp ikv \right) \Big|_{y=\pm a} = 0. \quad (2.6b)$$

A principal difficulty of the problem (2.5)–(2.6) is due to the need to consider this problem for the high frequency regime with  $\omega \geq 0.5$  GHz. Because the frequency  $\omega$  is large, the wave length  $\lambda = \text{Re}(2\pi/\omega)$  is very small, thus implying that  $\Omega$  should contain many wave lengths in both the  $x$  and  $y$  directions. On the other hand at least 10 grid points per wave length would be required for an accurate solution by, for example, the finite difference method. This would impose undesirable requirements for computer storage and CPU time if a conventional direct Gaussian elimination-like method for the factorization of the corresponding matrices were used. In addition, we must solve this problem for many values of  $\omega$  in order to generate the frequency-dependent data required for the inverse problem which motivates this study. Thus the issue of *rapid* algorithms becomes critical here. This has led us to develop a sophisticated iterative approach for the rapid solution of the above problem.

### 3. THE NUMERICAL METHOD

**3.1. Discretization.** We discretize the PDE (2.5) in the square  $\Omega$  by the five-point centered finite difference scheme with an uniform mesh cell size of  $h_x \times h_y$ , where  $h_x = 2a/M_x$ ,  $h_y = 2a/M_y$ , where  $M_x$  and  $M_y$  are the number of grid points in the  $x$  and  $y$  directions, respectively. Also, denote the maximum number of grid points across the target in the  $x$  direction by  $M_x^I$  and in the  $y$  direction by  $M_y^I$ . The gridded region uses  $x$  values from the interval  $[-a + h_x/2, a - h_x/2]$ , and  $y$  values from  $[-a + h_y/2, a - h_y/2]$ . The Sommerfeld-like boundary conditions (2.6) are imposed by use of a second order correct formula centered on each boundary, using fictitious values outside of  $\Omega$ , which are eliminated in setting up the matrix system. For example, on the right boundary ( $x = a$ ), the boundary conditions for some row  $j$  would be

$$\frac{v_{R,j} - v_{M_x,j}}{h_x} = ik_{M_x+1,j} \frac{v_{R,j} + v_{M_x,j}}{2},$$

where  $v_{R,j}$  is the fictitious value on the right.

Let  $k_{mj}^2$  be the matrix of (complex) values of the function  $k^2(x, y)$  on this grid, where the index  $m$  increases in the horizontal direction, and the index  $j$  increases in the vertical direction, and let  $k_{0j}^2$  be the vector of values of  $k_0^2(y_j)$  on the boundary of  $\Omega$  including  $y_0 = -a$  and  $y_{M_y+1} = a$ . Let  $f$  be the vector corresponding to the discretization of the right hand side  $f(x, y)$  of (2.5a). Then the corresponding linear system is  $A(v) = f$ , where the  $(M_x M_y) \times (M_x M_y)$  matrix  $A$  has the  $M_y$  by  $M_y$  block-tridiagonal form:

$$A = \begin{bmatrix} T_1 & -I & 0 & \cdots & 0 \\ -I & T_2 & -I & \cdots & 0 \\ \cdots & \cdots & \cdots & \cdots & \cdots \\ & & -I & T_{M_y-1} & -I \\ & & & -I & T_{M_y} \end{bmatrix}. \quad (3.1)$$

Here  $I$  is the identity matrix and the  $M_x \times M_x$  matrix  $T_j$  is given by

$$T_j = \left( 2 + 2 \frac{h_y^2}{h_x^2} \right) I - h_y^2 D_j - \frac{h_y^2}{h_x^2} B_j, \quad (3.2)$$

$$D_j = \text{diag}(k_{1,j}^2, k_{2,j}^2, \dots, k_{M_x,j}^2)$$

$$2 \leq j \leq M_y - 1.$$

The  $M_x \times M_x$  matrices  $B_j$  are defined as

$$B_j = \begin{pmatrix} \mu_j & 1 & 0 & \cdots & \cdots & 0 \\ 1 & 0 & 1 & 0 & \cdots & 0 \\ & & \ddots & & & \\ 0 & \cdots & 0 & 1 & 0 & 1 \\ 0 & \cdots & \cdots & 0 & 1 & \mu_j \end{pmatrix}, \quad (3.3)$$

where

$$\mu_j = 1 + \frac{ik_{0j}h_x}{1 - 0.5ik_{0j}h_x}.$$

For  $j = 1$  and  $j = M_y$  the  $M_x \times M_x$  matrix  $T_j$  in (3.2) has the form

$$T_j = \left( 1 - \frac{ik_{0l}h_y}{1 - 0.5ik_{0l}h_y} + 2\frac{h_y^2}{h_x^2} \right) I - h_y^2 D_j - \frac{h_y^2}{h_x^2} B_j, \quad (3.4)$$

where  $l = 0$  if  $j = 1$  and  $l = M_y + 1$  if  $j = M_y$ .

**3.2. Construction of a preconditioner.** Since  $A$  is large, sparse, and non-Hermitian, iterative methods using Krylov subspaces would seem feasible. A key issue for such accelerator methods is the successful creation of a preconditioning matrix  $A_N$ , to be used for example in the form

$$A \cdot A_N^{-1} w = f, \quad (3.5)$$

$$A_N v = w. \quad (3.6)$$

There are two somewhat conflicting requirements for  $A_N$ : The use of the inverse  $A_N^{-1}$  must be low cost, but effective enough to lead to a small number of iterations.

In our iterative algorithm we have developed a preconditioner by replacing the radiation boundary conditions at  $x = \pm a$  with Neumann boundary conditions and the variable coefficient  $k^2(x, y)$  with the constant (in  $x$ ) coefficient  $k_{0j}^2(y)$ , defined along the  $j$ th horizontal line of the grid. In this case the preconditioner  $A_N$  can be expressed in the form (3.1), in which, however, the matrices  $T_j$  have the simplified form

$$T_{N_j} = \left( 2 + 2\frac{h_y^2}{h_x^2} - h_y^2 k_{0j}^2 \right) I - \frac{h_y^2}{h_x^2} B, \quad (3.7a)$$

$$j = 2, \dots, M_y - 1$$

$$T_{N_j} = \left( 1 - \frac{ik_{0l}h_y}{1 - 0.5ik_{0l}h_y} + 2\frac{h_y^2}{h_x^2} - h_y^2 k_{0j}^2 \right) I - \frac{h_y^2}{h_x^2} B; \quad (3.7b)$$

$$j = 1 \text{ and } M_y,$$

where the values  $\mu_j$  in formulas (3.3) for the matrices  $B_j$  are changed to the constant 1 with  $B_j$  renamed simply  $B$ , and as earlier,  $l = 0$  if  $j = 1$  and  $l = M_y + 1$  if  $j = M_y$ .

The eigenvalues and eigenvectors of such matrices  $T_{N_j}$  are well known [25], as  $T_{N_j}$  differs from the real symmetric matrix  $B$  only by a constant diagonal matrix. It also follows that the resulting eigenvectors are orthogonal. The eigenvalues  $\lambda_s^j$  of the matrices  $T_{N_j}$  are

$$\lambda_s^j = 2 + 2\frac{h_y^2}{h_x^2} - h_y^2 k_{0j}^2 - 2\frac{h_y^2}{h_x^2} \cos\left(\frac{\pi(s-1)}{M_x}\right), \quad (3.8a)$$

$$\text{for } s = 1, \dots, M_x, \text{ and } j = 2, \dots, M_y - 1;$$

$$\lambda_s^j = 1 - \frac{ik_{0l}h_y}{1 - 0.5ik_{0l}h_y} + 2\frac{h_y^2}{h_x^2} - h_y^2 k_{0j}^2 - 2\frac{h_y^2}{h_x^2} \cos\left(\frac{\pi(s-1)}{M_x}\right), \quad (3.8b)$$

$$\text{for } s = 1, \dots, M_x, \text{ and } j = 1 \text{ and } M_y,$$

where  $l = 0$  if  $j = 1$  and  $l = M_y + 1$  if  $j = M_y$ .

For the eigenvalues  $\lambda_s^j$ , the corresponding eigenvectors are independent of  $j$ . These eigenvectors are  $\varphi^s = (\varphi_{s1}, \dots, \varphi_{sM_x})$ ,  $s = 1, \dots, M_x$ , where

$$\varphi_{sl} = \cos\left(\frac{\pi(s-1)(l-1/2)}{M_x}\right), \quad l = 1, \dots, M_x. \quad (3.9)$$

In the work below, assume that these eigenvectors have been normalized.

Therefore one can solve the system (3.6) by using a cosine transformation on each iteration of the GMRES method. We prefer, however, to work with the transformed system during the GMRES iterations. The advantage of the latter is that one can make the linear transformation only once, after the algorithm has converged.

Introduce the block diagonal matrices  $L$  and  $R$  as follows. Each diagonal block of the matrix  $L$  is the  $M_x \times M_x$  matrix  $\varphi_{sl}$ , and the diagonal block of matrix  $R$  is  $\varphi_{sl}^T$ . Now we can transform the system (3.5) as

$$R \cdot A \cdot A_N^{-1} L \bar{w} = \bar{f}, \quad (3.10a)$$

$$R \cdot A_N L \bar{v} = \bar{w}, \quad (3.10b)$$

where  $\bar{w} = R w$ ,  $\bar{f} = R f$ , and  $\bar{v} = R v$ .

Since  $\varphi^T * \varphi = I$  and  $\varphi^T * T_{N_j} * \varphi = \text{diag}(\lambda_1^j, \dots, \lambda_{M_x}^j)$ , the system (3.10b) has tridiagonal form and can be solved by a simple direct method. As an example, we accomplish this by explicitly computing the LU decomposition of the matrix  $RA_N L$  and using it to find the solution by the forward and backward substitutions at each iteration. The LU decomposition is based on Gaussian elimination with partial pivoting, and this approach is known to be stable in most practical problems. We have consistently observed this in our numerical experiments.

**3.3. Using a preconditioner as a solver.** Our preconditioner itself can be used as a solver. With  $RA_N L$  being the iterative matrix, this algorithm can be written as

$$RA_N L \bar{v}^{n+1} = \bar{f} - (RAL - RA_N L) \bar{v}^n, \quad (3.11)$$

where  $n$  is the iteration number. Convergence of (3.11) can be investigated by analyzing the spectrum of the matrix  $A_N^{-1} A$ . The complete numerical analysis of the spectrum of this matrix can be found in [13]. Also, we can use this information to investigate the convergence of GMRES, since the spectra of the left and right preconditioned matrices are the same. Unfortunately, however, in most calculations the algorithm (3.11) does not converge and it is necessary to replace the radiation boundary conditions with Neumann boundary conditions at  $x = \pm a$ . In this case satisfactory results are achieved only in the case of high, rather than low soil conductivity. A detailed description of this approach and comparison of the numerical results in the case of using Dirichlet, Neumann, and Sommerfeld boundary conditions can be found in [11].

**3.4. GMRES.** As we mentioned before, the application of the Krylov subspace method for the solution of the Helmholtz equation and radiation boundary conditions in [14] gave excellent results for the case of constant coefficients. We extend this approach to the case of non-constant coefficients. Because in the numerical experiments of [14] the number of iterations required for convergence was small, we chose to use the GMRES method instead of other variants. As will be seen in Section 4, this proved to be very successful.

This guaranties the calculations without the possible break downs of QMR used in [14]. In addition, if the number of iterations is small enough, it is not necessary to restart GMRES, which also makes the choice of this algorithm very attractive. Now, because some details of our numerical scheme differ from the common formulation of the GMRES [27], we describe below the sequence of steps for this algorithm:

1. Start: Cosine transformation of  $\bar{f} = Rf$
2. Choose  $\bar{w}_0$  and compute  $r_0 = \bar{f} - RAA_N^{-1}L\bar{w}_0 = \bar{f} - R(A_N + D)A_N^{-1}L\bar{w}_0$ ,  $y_1 = r_0/\|r_0\|$ ;
3. Iterate: For  $j = 1, 2, \dots, m$  do:

$$h_{i,j} = (RAA_N^{-1}Ly_j, y_i), \quad i = 1, 2, \dots, j$$

$$\hat{y}_{j+1} = RAA_N^{-1}Ly_j - \sum_{i=1}^j h_{ij}y_i$$

$$h_{j+1,j} = \|\hat{y}_{j+1}\|$$

$$y_{j+1} = \hat{y}_{j+1}/h_{j+1,j}$$

4. Form the approximate solution:

$$\bar{w}_m = \bar{w}_0 + \sum_{i=1}^m \alpha_i y_i,$$

where  $\alpha_m$  minimizes  $\|e_1\|r_0\| - H_m\alpha\|$ ,

where  $\alpha = (\alpha_1, \alpha_2, \dots, \alpha_m)$ ,  $e_1$  is a first column of the  $(k+1) \times (k+1)$  identity matrix,  $H$  is a  $(k+1) \times k$  Hessenberg matrix.

5. Find the solution by the inverse transform  $v_m = Lw_m$ .

A convergence analysis of GMRES-type algorithms can be found in [13, 24].

In our case the preconditioner  $A_N$  and the matrix  $A$  differ by a matrix of rank  $l \leq 2M_y + M_x^l M_y^l$  and one can prove then that at least  $M_x M_y - 2M_y - M_x^l M_y^l$  eigenvalues of the preconditioned matrix are identically one. The convergence GMRES was studied in a variety of publications. Such estimations, where the majority of the eigenvalues (the last  $M_x M_y - l$  eigenvalues) were close to 1, were considered in [24]. These estimations are based on the analysis of  $\max\{|\lambda_i - \lambda_j|, i \leq j \leq l\}/|\lambda_i|$ . So, it is important to know the distribution of the first  $l$  eigenvalues of the preconditioned matrix. An effective numerical procedure for this analysis was proposed in [13]. To rapidly solve the problems (2.5), (2.6) for many frequencies, we have used an extrapolation from several previous frequencies as a first approximation for the next one. Specifically we used extrapolation formulas from 1st to 4th order. We will report on the effectiveness of this approach in the next section.

#### 4. NUMERICAL RESULTS

The above algorithm was implemented in FORTRAN 77 using complex double precision arithmetic on a Silicon Graphics Origin 200, using one processor. In the tests below the geometrical sizes are given in meters. The ranges of the parameters  $\omega$ ,  $\epsilon_r$ , and  $\tan(\delta)$  are as in [8, 26]. We choose the frequency range to be  $\omega \in (0.5, 2)$  GHz. For this choice of frequencies we obtain the following values of the electrical properties:

**TABLE I**  
**Electrical Parameters**

	$\varepsilon_r$	$\tan(\delta)$	$k^2(\omega = 1 \text{ GHz})$
Air	1	0	439.2
Dry soil	2.9	0.025	$1273 + 31i$
Wet soil (5% moisture)	4	0.22	$1756 + 395i$
TNT	2.86	0.0018	$1256 + 2.26i$

$$\mu = 4\pi \times 10^{-7} \frac{\text{Henry}}{m},$$

$$\varepsilon_0 = 8.854 \times 10^{-12} \frac{\text{Farad}}{m}.$$

The values of the electrical parameters in Table I are taken from [26]; the values of  $k^2$  are non-dimensional.

*4.1. Two tests verifying convergence on a model problem.* In the first two tests we consider the convergence of the algorithm on a sequence of grids. The source function  $f$  was selected such that the true solution was  $v(x, y) = \phi(x) \cdot \phi(y)$ , where  $\phi(x) = \exp(ik_0(x + a)) + \exp(-ik_0(x - a)) - 2$ . Note that the analytic solution satisfies the radiation boundary condition (2.6). The error is *reported* as the relative maximum norm  $r_\infty^n = \|V^{(n)} - v\|_\infty / \|v\|_\infty$ , and the iterative process is stopped when the *initial* residual is reduced by a factor of  $10^{-7}$ . Actually in our numerical experiments it would have been sufficient to stop the algorithm when the initial residual is reduced by  $10^{-5}$ , because after this value was achieved, the difference between the analytic and numerical solution remained essentially the same. In these experiments we used the domain  $\Omega = (-50 \text{ cm}, 50 \text{ cm})^2$  and zero initial values were assumed. In the reportage of this section  $N_0$  is the iteration number when the convergence criteria was first satisfied and TP is the total time in seconds.

In Table II, we report on the numerical results for the propagation of waves in a non-attenuating media, i.e.,  $k^2 \equiv 439.2$ . It should be noticed that the number of iterations holds roughly constant as the mesh size  $h$  decreases, a behavior similar to multigrid at its best. This has important advantages for large-scale problems.

Next, we consider a case using an uniform background (without interface) with two inclusions. The parameters of the background in this test correspond to dry soil, where  $k^2 = k_0^2$  outside of two circular abnormalities, one of which models a mine and the other an air gap. The radius of each abnormality is 5 cm. The distribution of  $k^2$  in the first inclusion corresponds to TNT (trinitrotoluene) and in the second inclusion  $k^2$  corresponds to air. Thus

**TABLE II**  
**Results of Numerical Experiments for the First Test**

Grid	$r_\infty^{(n)}$	$N_0$	TP (s)
$99 \times 99$	$9.89 \times 10^{-3}$	7	0.5
$199 \times 199$	$2.61 \times 10^{-3}$	8	2.2
$399 \times 399$	$6.73 \times 10^{-4}$	8	9.8

**TABLE III**  
**Results of Numerical Experiments for the Second Test**

Grid	$r_{\infty}^{(n)}$	$N_0$	$TP$ (s)
99 × 99	$9.96 \times 10^{-3}$	11	0.6
199 × 199	$2.60 \times 10^{-3}$	11	2.7
399 × 399	$6.73 \times 10^{-4}$	11	10

$k^2$  can be represented in the form

$$k^2 = \begin{cases} 1273 + 31i, & \text{for } (x - x_i)^2 + (y - y_i)^2 > r_i^2, \quad i = 1, 2 \\ 1256 + 2.26i, & \text{for } (x - x_1)^2 + (y - y_1)^2 \leq r_1^2, \\ 439, & \text{for } (x - x_2)^2 + (y - y_2)^2 \leq r_2^2, \end{cases} \quad (4.1)$$

where  $(x_1, y_1) = (0, 15)$  cm,  $(x_2, y_2) = (0, 40)$  cm, and  $r_{1,2} = 5$  cm are the centers and radii of the first and second inclusions, respectively.

We see several interesting results from Table III: The method converges rapidly, in each case always taking just 11 iterations/run. The CPU time is roughly proportional to the number of unknowns. Again, the error is clearly 2nd order as should be expected.

**4.2. A target in wet soil containing TNT.** In the third series of tests we compute the response to a mine-like target (TNT) in wet soil. We use ranges of parameters as above. Mine-like targets were embedded within  $\Omega \cap \{y > 0\}$ . The domain  $\Omega \cap \{y < 0\}$  consists of dry air. We choose the function  $k^2$  as

$$k^2(x, y) = \begin{cases} 439.2, & \text{for } y < 0 \\ 1756 + 395i, & \text{for } y > 0, (x - x_1)^2 + (y - y_1)^2 > r_1^2 \\ 1256 + 2.26i, & \text{for } (x - x_1)^2 + (y - y_1)^2 \leq r_1^2 \end{cases} \quad (4.2)$$

where  $x_1 = 0$ ,  $y_1 = 20$  cm,  $r_1 = 5$  cm.

Hence the first two rows in (4.2) correspond to  $k_0^2$ , and the third one is due to a mine-like target, which we model as a circle with center at  $(x_1, y_1) = (0, 20)$  cm, and with radius  $r_1 = 5$  cm. The values of the parameter  $k_0^2$  correspond to air for  $y < 0$  and to 5% moisturized sand for  $y > 0$ . The frequency  $\omega = 1$  GHz was chosen here. The value of the parameter  $k^2$  within the target corresponds to trinitrotoluene (TNT) (see Table I). In all cases 19 iterations were required for convergence, without regard to details.

Figures 2 and 3 show a contour plot of the amplitude and phase over the domain  $(-106 \text{ cm}, 106 \text{ cm})^2$  using a computational grid of size  $399 \times 399$ . Horizontal lines at the detector region  $y = -10$  and the interface line  $y = 0$  were added, as an aid to interpretation. In these two plots we made an exception to our usual convention, and placed air in the upper half plane. In addition a circle was drawn in the soil showing the land mine. In the amplitude contour plot, two levels of contour lines were used: One fine set for the very small amplitudes away from the land mine, and one coarse set for the region near the land mine, where there is rapid growth. The phase contour plot shows many interesting features and structures. The phase changes from  $-\pi$  to  $\pi$  radians between each set of dark bands, which are roughly centered at the land mine. The bands are wider in the air and narrower

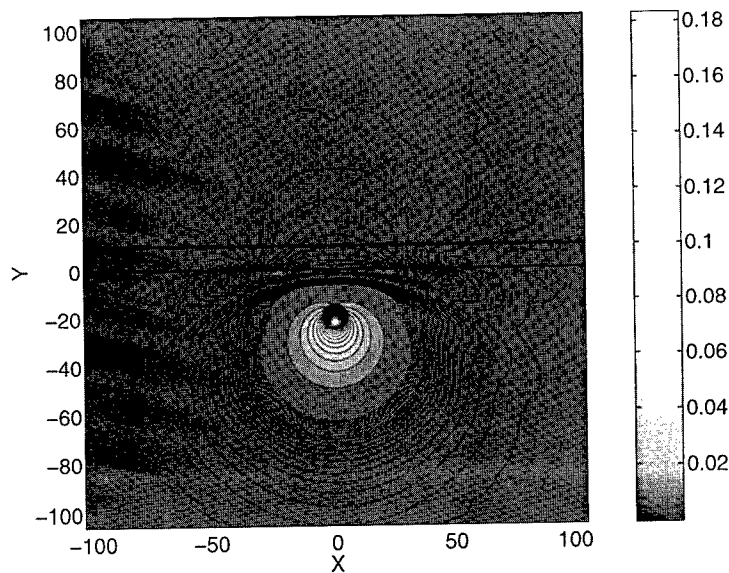


FIG. 2. Contour plot of the amplitude of the function  $v$  in Test 3 at 1 GHz.

in the soil. Two new bands begin near the interface and go into the soil. Examination of a larger domain (not shown) shows that additional bands such as these were not generated, but other structures emerged. We have found the systematic structure of these contours to be most interesting.

One important issue in the numerical solution of scattering problems is the influence of the size of the computational domain on the quality of the solution. To ensure the accuracy of the solution we should verify that the size of the computational domain does not change the solution in the region of the interest, after a certain size. To examine this

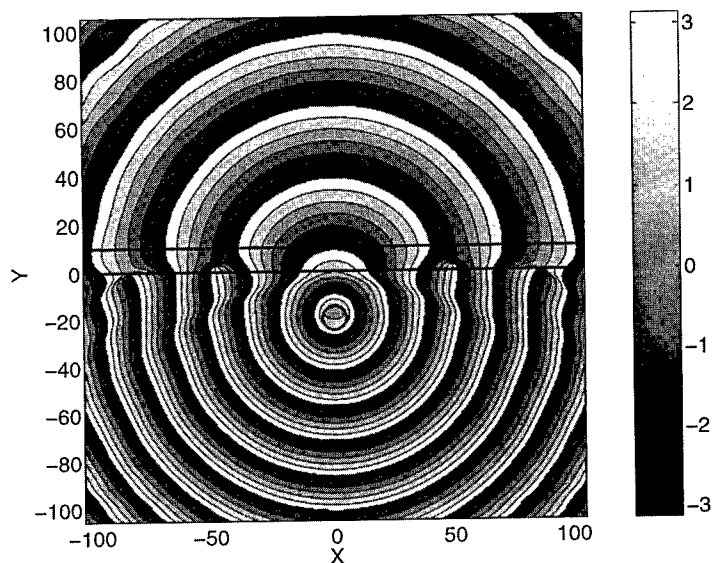
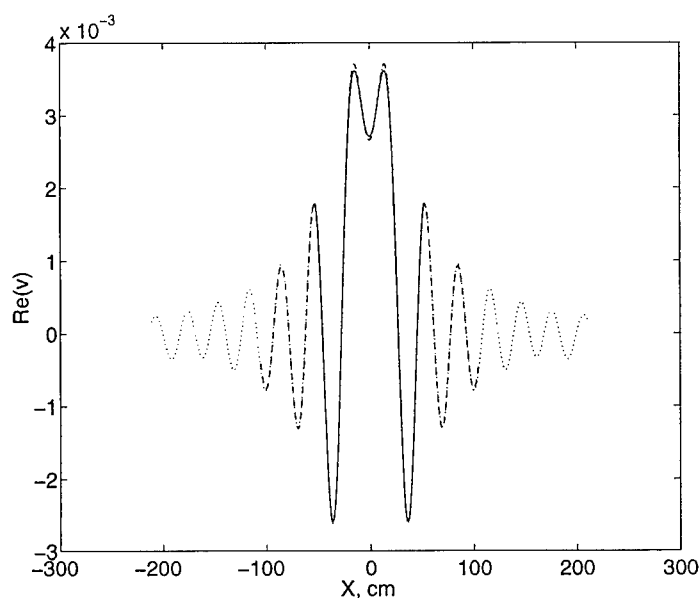
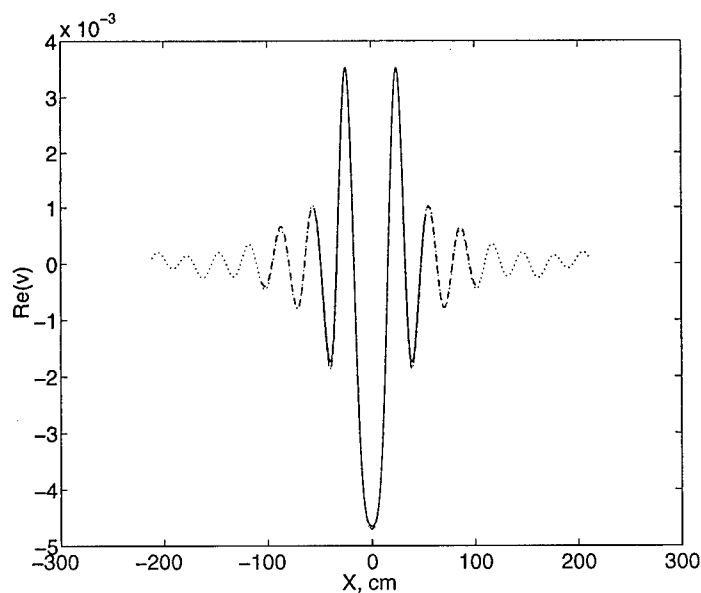


FIG. 3. Contour plot of the phase in radians of the function  $v$  in Test 3 at 1 GHz.



**FIG. 4.** The  $x$ -dependent distribution of the real part of the function  $v$  for Test 3 at the level  $y = -10$  (i.e., 10 cm above the air-ground interface). The solid, dashed, and dotted lines display the cases of  $\{-53 \leq x, y \leq 53\}$  cm,  $\{-106 \leq x, y \leq 106\}$  cm, and  $\{-212 \leq x, y \leq 212\}$  cm domains, respectively.

we considered 3 different computational domains  $(-53 \text{ cm}, 53 \text{ cm})^2$ ,  $(-106 \text{ cm}, 106 \text{ cm})^2$ ,  $(-212 \text{ cm}, 212 \text{ cm})^2$ , using grid sizes of  $199 \times 199$ ,  $399 \times 399$ , and  $799 \times 799$ , respectively. The parameters of the background and the inclusion as well as the position of the inclusion were fixed. Figures 4 and 5 display the distribution of the real part of the function  $v$  10 cm above the ground surface and at the ground surface ( $y = -10, 0.0$  cm). One can observe



**FIG. 5.** Similar to Fig. 3, but at the level  $y = 0$  (i.e., on the air-ground interface).

the excellent agreement between these distributions over the smallest comparison region  $[-53 \text{ cm}, 53 \text{ cm}]$ : There is a slight difference at the inner peaks for the smallest computational domain, but agreement over the next two domains. Similar plots were obtained for the imaginary parts of the function  $v$ . Comparison of both real and imaginary parts for regions in the ground, such as  $y = 10$  or  $20 \text{ cm}$ , shows exact agreement, to graphical accuracy, and increasing values for the peaks.

**4.3. A target in wet soil containing a mixture of TNT and air.** The goal of the fourth test was to compute the *frequency dependent* response for detectors placed on the ground for two different types of mine-like targets. Recall that we need such a response as an input for the solution of the inverse problem. It is well known that air often composes from 10 to 30% of a mine. The rest of a plastic mine is a TNT-like explosive. So, one can hope that an air signature in this output signal might help to differentiate mines from clutter. Therefore we simulate two mine-like targets. The first was a circle with radius  $r = 5 \text{ cm}$  filled with TNT and with center  $x_1 = 0, y_1 = 20 \text{ cm}$ , i.e., the same as in the second test. The second target consists of two concentric circles with the same center of  $(0, 20) \text{ cm}$ . The radius of the first circle was  $r_1 = 4 \text{ cm}$ , and the radius of the second was  $r_2 = 5 \text{ cm}$ . The first circle was filled with TNT, and the annulus between the first and second circles consisted of dry air. We computed the boundary value problem (3.2), (3.3a), (3.5) for the frequencies  $\omega \in (0.5, 2) \text{ GHz}$  with the step size  $\Delta\omega = 0.01 \text{ GHz} = 10 \text{ Mhz}$ , thus solving 150 problems. The total time was 5 minutes using a  $199 \times 199$  grid. At each frequency  $\omega$  the initial distribution for the function  $v$  was taken as an extrapolation from the solutions at the previous frequencies. To do this, we considered extrapolation formulas of different orders. Figure 6 shows the distribution of the number of iterations for different frequencies using zero as the initial approximation, as well as for 1st, 2nd, 3rd, and 4th order extrapolation formulas. Note that for the 4th order extrapolation formula, only 9–11

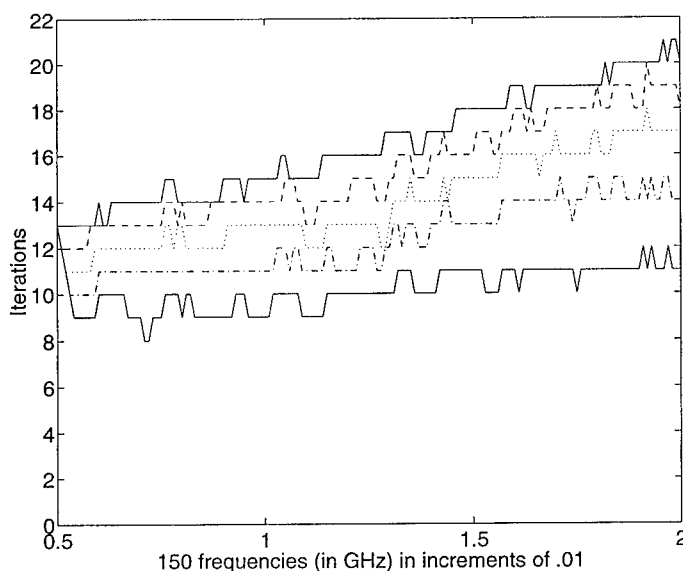


**FIG. 6.** The number of iterations for extrapolation formulas of different orders, as a function of frequency. The top solid line uses an initial approximation of zero. The dashed, dotted, dot-dashed, and bottom solid lines represent the improvements achieved by use of 1st, 2nd, 3rd, and 4th extrapolation formulas for the initial approximation.

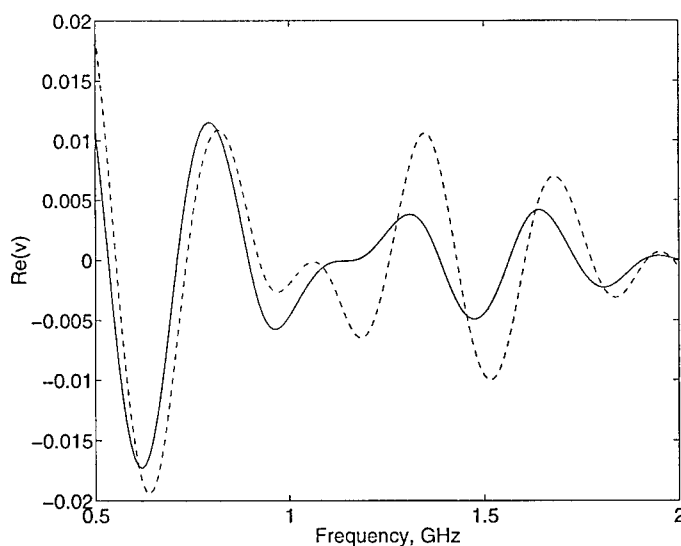


**FIG. 7.** Frequency dependent distribution of the real part of the function  $v(x, y, \omega)$ . The solid and dashed line display responses from TNT filled and air-TNT filled targets at a detector location of  $(x, y) = (0, -10)$  cm. The difference in responses, especially from 1 to 1.6 GHz is evident.

iterations were required in most cases, in contrast to requiring up to 20 without use of extrapolation.

Figure 7 displays the resulting frequency dependent curves at  $x = 0, y = -10$ , at a detector placed 10 cm above the air-ground interface and just above the center of the target. Solid and dashed lines correspond to TNT-filled and air-TNT filled targets, respectively. The difference in the two responses is evident, especially between 1 and 1.6 GHz. Figure 8 shows similar curves but for a detector which is located at  $(x, y) = (10, -10)$  cm, i.e., 10 cm to the right of the previous detector. Again a similar difference in responses can be

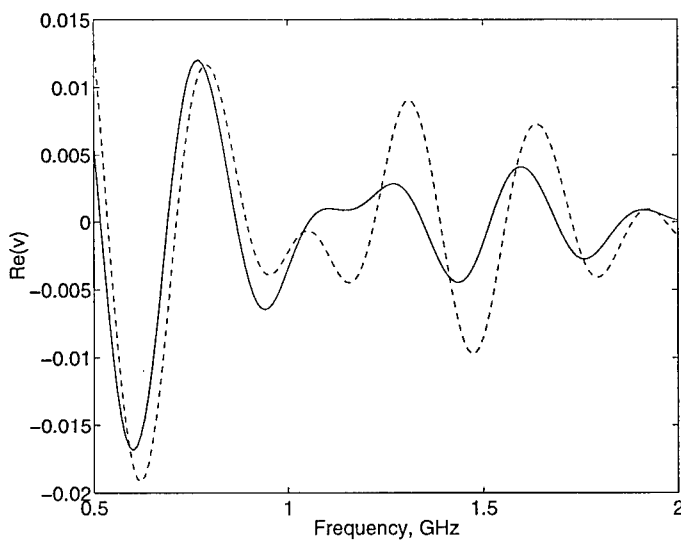


**FIG. 8.** The same as in Fig. 5, but at a detector location of  $(x, y) = (10, -10)$  cm.

observed. However, beginning from about  $x = 30$  cm such differences are very small (these results are not shown).

## 5. CONCLUSIONS

A new and rapid iterative method for the solution of the forward problem of propagation of high frequency GPR signals using Sommerfeld-like boundary conditions over regions with small inclusions was developed and computationally implemented. A typical time to produce the frequency dependent response over 150 frequencies on a  $199 \times 199$  grid was just 5 minutes on a Silicon Graphics Origin 200 using only one processor, as contrasted to about 6 hours in the case of Gaussian elimination like methods.

The method was tested for realistic parameter ranges. The influence of the truncated region on the numerical solution of the scattered problem for the Helmholtz equation with Sommerfeld-like boundary conditions was investigated. Interesting features of the amplitude and phase distribution were shown and reported. It was found that the frequency dependent output signals for two types of mine-like targets, (1) one filled only with the TNT, and (2) one filled with both TNT and dry air, were significantly different. Given that mines contain from 10 to 30% of air, and stone-like clutter likely does not contain air, this may well help to differentiate mines from clutter (along with other similar parameters). The authors intend to use the developed code to simulate data for the inverse problem, which will be solved by the elliptic systems method [10, 19, 20].

## ACKNOWLEDGMENT

This material is based upon work supported by the U.S. Army Research Office Grant DAAG 55-98-1-0401.

## REFERENCES

1. A. Bayliss, C. Goldstein, and E. Turkel, An iterative method for the Helmholtz equation, *J. Comput. Phys.* **49**, 443 (1983).
2. J. Berenger, A perfect matched layer for the absorption of electromagnetic waves, *J. Comput. Phys.* **114**, 185 (1994).
3. J. H. Bramble, J. E. Pasciak, and J. Xu, The analysis of multigrid algorithms for non-symmetric and indefinite problems, *Math. Comp.* **51**, 389 (1988).
4. B. L. Buzbee, F. W. Dorr, J. A. George, and G. H. Golub, The direct solution of the discrete Poisson equation on irregular regions, *SIAM J. Numer. Anal.* **8**, 722 (1971).
5. B. L. Buzbee, G. H. Golub, and C. W. Nelson, On direct methods for solving Poisson's equation, *SIAM J. Numer. Anal.* **7**, 627 (1970).
6. M. Cheney and D. Isaacson, Inverse problems for a perturbed dissipative half-space, *Inverse Problems* **11**, 865 (1995).
7. B. Despres, Domain decomposition method and the Helmholtz problem, in *Mathematical and Numerical Aspects of Wave Propagation Phenomena*, edited by G. Gohén, L. Halpern, and P. Joly (SIAM, Philadelphia, 1991), p.44.
8. *Dielectric Constant and Loss Tangent of Explosives*, data of U.S. Army Belvoir RD&E Center (unpublished).
9. J. Douglas, Jr., J. L. Hensley, and J. E. Roberts, *Alternating-Direction Iteration Method for Helmholtz Problems*, Tech. Report No. 214, Mathematics Department, Purdue University, West Lafayette, IN, 1993.
10. Y. A. Gryazin, M. V. Klibanov, and T. R. Lucas, Imaging the diffusion coefficient in a parabolic inverse problem in optical tomography, *Inverse Problems* **15**, 373 (1999).

11. Y. A. Gryazin, M. V. Klibanov, and T. R. Lucas, Tomographic images of land mines by the elliptic systems method using GPR: Efficient solution of the forward problem, in *Proc. of the International Society of Optical Engineering (SPIE), Detection and Remediation Technologies for Mines and Minelike Targets IV* (1999), Vol. 3710, p.875.
12. H. C. Elman and D. P. O'Leary, Efficient iterative solution of the three-dimensional Helmholtz equation, *J. Comput. Phys.* **142**, 163 (1998).
13. H. C. Elman and D. P. O'Leary, Eigenanalysis of some preconditioned Helmholtz problems, *Numer. Math.* **83**, 231 (1998).
14. O. Ernst and G. H. Golub, A domain decomposition approach to solving the Helmholtz equation with a radiation boundary condition, in *Domain Decomposition in Science and Engineering*, edited by A. Quarteroni, H. Periaux, Y. Kuznetsov, and O. Widdlund (Amer. Math. Soc., Providence, 1994), p.177.
15. W. Joubert, T. A. Manteuffel, S. V. Parter, and S.-P. Wong, Preconditioning second-order elliptic operators: Experiment and theory, *SIAM J. Sci. Statist. Comput.* **13**, 259 (1992).
16. M. Kilmer, E. Miller, and C. Rappaport, Preconditioners for structured matrices arising in subsurface object detection, *SIAM J. Sci. Comput.*, in press.
17. S. Kim, A parallizable iterative procedure for the Helmholtz problem, *Appl. Numer. Math.* **14**, 435 (1994).
18. S. Kim, Parallel multidomain iterative algorithms for the Helmholtz wave equation, *Appl. Numer. Math.* **17**, 411 (1995).
19. M. V. Klibanov, T. R. Lucas, and R. M. Frank, A fast and accurate imaging algorithm in optical/diffusion tomography, *Inverse Problems* **13**, 1341 (1997).
20. M. V. Klibanov, T. R. Lucas, and R. M. Frank, Image reconstruction from experimental data in diffusion tomography, in *Computational Radiology and Imaging, Theory and Diagnostics*, edited by C. Börgers and F. Natterer, The IMA Volumes in Mathematics and Its Applications (Springer-Verlag, New York/Berlin, 1999), Vol. 110, p.157.
21. T. A. Manteuffel and S. V. Parter, Preconditioning and boundary conditions, *SIAM J. Numer. Anal.* **27**, 656 (1998).
22. E. Marengo, C. Rappaport, and E. Miller, Optimum PML ABC conductivity profile in FDFD, submitted for publication.
23. N. M. Nachtigal, S. C. Reddy, and L. N. Trefethen, How fast are nonsymmetric matrix iterations, *SIAM J. Matrix Anal. Appl.* **13**, 778 (1992).
24. C. W. Oosterlee and T. Washio, An evaluation of parallel multigrid as a solver and a preconditioner for singularly perturbed problems, *SIAM J. Sci. Comput.* **19**, 87 (1998).
25. W. Proskurowski and O. Widlund, On the numerical solution of Helmholtz' equation by the capacitance matrix method, *Math. Comp.* **30**, 433 (1976).
26. *Permittivity and Conductivity for Sandy Loam for Various Moistures*, data of U.S. Army Belvoir RD&E Center (unpublished).
27. Y. Saad and M. H. Schultz, GMRES: A generalized minimal residual algorithm for solving nonsymmetric linear systems, *SIAM J. Sci. Statist. Comput.* **7**, 856 (1986).

REPORT DOCUMENTATION PAGE			Form Approved OMB NO. 0704-0188	
Public reporting burden for this collection of information is estimated to average 1 hour per response, including the time for reviewing instructions, searching existing data sources, gathering and maintaining the data needed, and completing and reviewing the collection of information. Send comment regarding this burden estimates or any other aspect of this collection of information, including suggestions for reducing this burden, to Washington Headquarters Services, Directorate for Information Operations and Reports, 1215 Jefferson Davis Highway, Suite 1204, Arlington, VA 22202-4302, and to the Office of Management and Budget, Paperwork Reduction Project (0704-0188), Washington, DC 20503.				
1. AGENCY USE ONLY (Leave blank)		2. REPORT DATE		3. REPORT TYPE AND DATES COVERED Reprint
4. TITLE AND SUBTITLE  Title on Reprint			5. FUNDING NUMBERS  DAAG55-98-1-0401	
6. AUTHOR(S)  Authors on Reprint				
7. PERFORMING ORGANIZATION NAMES(S) AND ADDRESS(ES)  University of North Carolina at Charlotte Charlotte, NC 28223			8. PERFORMING ORGANIZATION REPORT NUMBER	
9. SPONSORING / MONITORING AGENCY NAME(S) AND ADDRESS(ES)  U.S. Army Research Office P.O. Box 12211 Research Triangle Park, NC 27709-2211			10. SPONSORING / MONITORING AGENCY REPORT NUMBER  ARO 38897.3-MA-LMD	
11. SUPPLEMENTARY NOTES  The views, opinions and/or findings contained in this report are those of the author(s) and should not be construed as an official Department of the Army position, policy or decision, unless so designated by other documentation.				
12a. DISTRIBUTION / AVAILABILITY STATEMENT  Approved for public release; distribution unlimited.			12 b. DISTRIBUTION CODE	
13. ABSTRACT (Maximum 200 words)  ABSTRACT IN REPRINT				
14. SUBJECT TERMS			15. NUMBER IF PAGES	
			16. PRICE CODE	
17. SECURITY CLASSIFICATION OF REPORT UNCLASSIFIED	18. SECURITY CLASSIFICATION OF THIS PAGE UNCLASSIFIED	19. SECURITY CLASSIFICATION OF ABSTRACT UNCLASSIFIED	20. LIMITATION OF ABSTRACT  UL	